CCD Photometry, Light Curve Modeling, and Period Study of the Overcontact Binary Systems V647 Virginis and V948 Monocerotis

Kevin B. Alton
UnderOak Observatory, 70 Summit Avenue, Cedar Knolls, NJ 07927; mail@underoakobservatory.com

Received December 27, 2018; revised February 19, March 26, 2019; accepted May 2, 2019

Abstract Prior to this investigation, monochromatic CCD data for V647 Vir and V948 Mon had only been generated from automated surveys which employ sparse sampling strategies. In this study precise multi-color (B, V, and I_c) light curve data for V647 Vir (2018) and V948 Mon (2017–2018) were acquired at Desert Bloom Observatory (DBO). Both targets produced new times of minimum which were used along with other eclipse timings from the literature to update their corresponding ephemerides. Despite the limited amount of published data, preliminary evidence suggests a secular decrease in the orbital period of V948 Mon. Roche modeling to produce synthetic fits to the observed light curve data was accomplished using the Wilson-Devinney code. Since each system exhibits a total eclipse, a reliable value for the mass ratio (q) could be determined leading in turn to initial estimates for the physical and geometric elements of both variable systems.

1. Introduction

CCD-derived photometric data for V647 Vir (NSVS 13280611; GSC 00314-00388) were first acquired from the ROTSE-I survey between 1999–2000 (Akerlof *et al.* 2000; Wozniak *et al.* 2004; Gettel *et al.* 2006) and later from the Catalina Sky Survey (Drake *et al.* 2014). Its classification as a W UMa variable was assigned according to Hoffman *et al.* (2009). The variability of V948 Mon (GSC 04846-00809) was initially observed from data collected (1994–1996) in a calibration field for the Sloan Digital Sky Survey (Henden and Stone 1998) and later confirmed by Greaves and Wils (2003). Sparsely sampled photometric data for V948 Mon were also acquired from the ROTSE-I, ASAS (Pojmański *et al.* 2005), and Catalina surveys. Although other times of minimum light have been sporadically published, this paper marks the first detailed period analysis and multi-color Roche model assessment of light curves (LC) for V647 Vir and V948 Mon.

2. Observations and data reduction

Time-series images were acquired at Desert Bloom Observatory (DBO, USA—110.257 W, 31.941 N) with an SBIG STT-1603ME CCD camera mounted at the Cassegrain focus of a 0.4-m f/6.8 catadioptric telescope. This instrument produces an image scale of 1.36 arcsec / pixel (bin = 2 × 2) and a field of view (FOV) of 11.5' × 17.2'. Image acquisition (75-s) was performed using MAXIM DL v.6.13 (Diffraction Limited 2019) or THESKYX PRO v.10.5.0 (Software Bisque 2019). The CCD-camera is equipped with B, V, and I_c filters manufactured to match the Johnson-Cousins Bessell prescription. Dark subtraction, flat correction, and registration of all images collected at DBO were performed with AIP4WIN v.2.4.0 (Berry and Burnell 2005). Instrumental readings were reduced to catalog-based magnitudes using the APASS star fields (Henden *et al.* 2009, 2010, 2011 and Smith *et al.* 2011) built into MPO CANOPUS v.10.7.1.3 (Minor Planet Observer 2010). In order to minimize any potential error due to differential refraction and color extinction only data from images taken above 30° altitude (airmass < 2.0) were included.

3. Results and discussion

LCs for V647 Vir and V948 Mon were generated using an ensemble of five non-varying comparison stars in each FOV. The identities, J2000 coordinates, V-mags, and APASS color indices (B–V) for these stars are listed in Table 1. Uncertainty in comparison star measurements made in the same FOV with V647 Vir or V948 Mon typically stayed within ± 0.007 mag for V- and I_c- and ± 0.010 mag for B-passbands.

3.1. Photometry and ephemerides

Times of minimum were calculated using the method of Kwee and van Woerden (1956) featured in PERANSO v.2.5 (Paunzen and Vanmunster 2016; Vanmunster 2018). Long-term or secular changes in orbital period can sometimes be revealed by plotting the difference between the observed eclipse times and those predicted by a reference epoch against cycle number. Curve fitting all eclipse timing differences (ETD) was accomplished using scaled Levenberg-Marquardt algorithms. The results from these analyses are separately discussed for each binary system in the subsections below.

3.1.1. V647 Vir

A total of 334 photometric values in B-, 350 in V-, and 333 in I_c-passbands were acquired from V647 Vir between January 25, 2018 and March 19, 2018. Included in these determinations were seven new times of minimum (ToM) which are summarized in Table 2. Photometric data from the NSVS (1999–2000) and ASAS (2001–2009) surveys were folded together with V-mag data generated at DBO (2018). This was accomplished by applying periodic orthogonals (Schwarzenberg-Czerny 1996) to fit observations and analysis of variance to assess fit quality (PERANSO v.2.5; Paunzen and Vanmunster 2016; Vanmunster 2018). Despite significant scatter in the survey data, near congruence of the light curves was observed when P = 0.3478960 d (Figure 1). NSVS and ASAS timings contained within the uncertainty calculated (Kwee and van Woerden 1956) for the midpoint of the folded LCs during Min I and Min II were added to the list of ToM values summarized in Table 2. These results (n = 2) along with other published eclipse timings

Table 1. Astrometric coordinates (J2000), V-mags, and color indices (B–V) for V647 Vir, V948 Mon, and their corresponding five comparison stars used in this photometric study.

Star Identification	*R.A. (J2000)* *h m s*	*Dec. (J2000)* *° ′ ″*	*V-mag*[a]	*(B–V)*[a]
V647 Vir	13 47 51.86	+07 00 45.79	12.603	0.725
GSC 00314-00627	13 47 24.50	+06 54 32.22	11.732	0.696
GSC 00314-00198	13 47 39.99	+06 52 37.88	12.101	0.743
GSC 00314-00530	13 47 55.13	+06 54 27.90	13.744	0.746
GSC 00314-00282	13 47 57.83	+07 04 50.99	12.814	0.854
GSC 00314-00009	13 47 44.60	+07 04 18.31	10.487	1.031
V948 Mon	08 01 51.19	-00 33 26.27	13.184	0.471
GSC 04846-00921	08 01 37.94	–00 38 31.38	12.653	0.506
GSC 04846-00463	08 01 19.32	–00 36 42.52	13.437	0.572
GSC 04846-02159	08 01 31.56	–00 37 38.89	13.528	0.611
GSC 04846-00795	08 01 30.12	–00 36 19.76	13.280	0.514
GSC 04846-01147	08 01 48.35	–00 28 24.17	13.179	0.509

a. V-mag and (B–V) for comparison stars derived from APASS database described by Henden et al. *(2009, 2010, 2011) and Smith* et al. *(2011), as well as on the AAVSO web site (https://www.aavso.org/apass).*

Table 2. V647 Vir times-of-minimum (February 2, 2000–March 19, 2018), cycle number, and residuals (ETD) between observed and predicted times derived from the updated linear ephemeris (Equation 2).

HJD 2400000+	*HJD Error*	*Cycle No.*	*ETD*[a]	*Reference*
51604.0046	0.0018	–18951	0.00023	NSVS[b]
54585.6480	0.0009	–10380.5	0.00069	ASAS[b]
54948.6773	0.0006	–9337	0.00048	Diethelm 2009
54948.8499	0.0001	–9336.5	–0.00087	Diethelm 2009
55634.9009	0.0001	–7364.5	–0.00084	Diethelm 2011
55687.7813	0.0002	–7212.5	–0.00064	Diethelm 2011
56000.8888	0.0002	–6312.5	0.00043	Diethelm 2012
58143.9284	0.0001	–152.5	0.00046	This study
58144.9712	0.0002	–149.5	–0.00039	This study
58146.0155	0.0001	–146.5	0.00021	This study
58156.9745	0.0002	–115	0.00049	This study
58184.9804	0.0001	–34.5	0.00072	This study
58196.8080	0.0002	–0.5	–0.00014	This study
58196.9812	0.0003	0	–0.00085	This study

a. ETD = Eclipse Time Difference between observed time-of-minimum and predicted values using the updated ephemeris (Equation 2).
b. Estimated following superimposition of NSVS, ASAS, and DBO (2018) lightcurves when folded at P = 0.3478960 d.

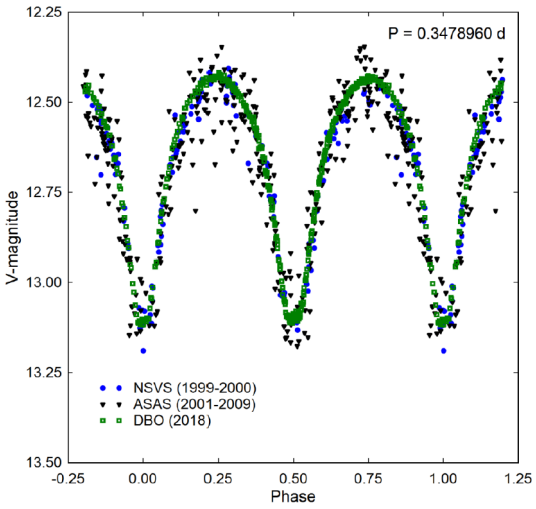

Figure 1. Period folded (P = 0.3478960 d) LCs for V647 Vir produced from NSVS, ASAS, and DBO photometric data. NSVS and ASAS LCs were offset to match the V-mag values determined from precise CCD photometry performed at DBO.

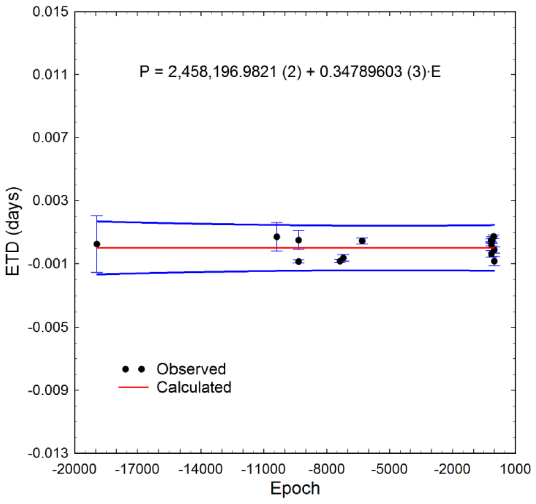

Figure 2. Eclipse timing differences (ETD) vs. epoch for V647 Vir calculated using the updated linear ephemeris (Equation 2). Measurement uncertainty is demarked by the hatched vertical lines. The solid red line indicates the linear fit while the blue lines represent the 95% confidence intervals which include the zero intercept.

from 1999 through 2017, were used to initially calculate ETD values with the reference epoch (Kreiner 2004) defined by the following linear ephemeris (Equation 1):

$$\text{Min I (HJD)} = 2454506.847 + 0.347896\ E. \quad (1)$$

An updated linear ephemeris (Equation 2) was thereafter derived as follows:

$$\text{Min I (HJD)} = 2458196.9821\ (2) + 0.34789603\ (3)\ E \quad (2)$$

It should be noted that eclipse timing data for V647 Vir are only available for the past 18 years with large time gaps between 2001–2008 and 2012–2018. The residuals (ETD) which are best described by a straight-line fit indicate that no substantive change in the orbital period has occurred since 2000 (Figure 2). Not surprisingly given the paucity of data, no other underlying variations in the orbital period stand out, such as those that might be caused by the magnetic cycles (Applegate 1992) or the presence of an additional gravitationally bound stellar-size body.

3.1.2. V948 Mon

A total of 604 photometric values in B-, 379 in V-, and 381 in I_c-passbands were acquired from V948 Mon between December 23, 2017 and January 5, 2018. Included in these determinations were seven new ToM values which are provided in Table 3. These data along with other published results were used to initially analyze eclipse timings according to the

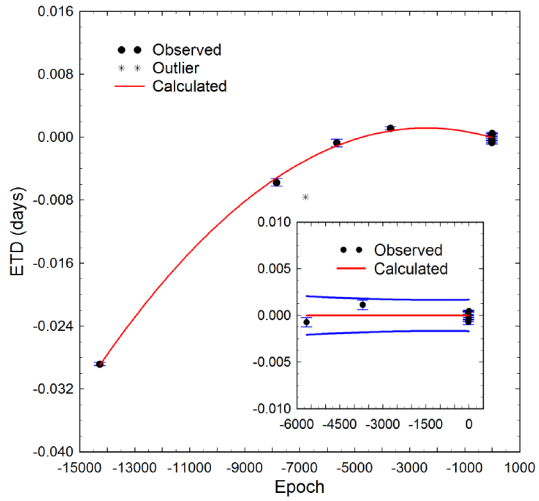

Figure 3. The downwardly directed quadratic fit to the ETD vs. epoch data (Equation 4) is shown with a solid red line and suggests the orbital period of V948 Mon is decreasing with time. The inset panel shows the near-term data which produced the updated linear ephemeris (Equation 5). Measurement uncertainty is demarked by the hatched vertical lines. The solid red line indicates the linear fit while the blue lines represent the 95% confidence intervals which include the zero intercept.

Table 3. V948 Mon times of minimum (April 13, 2003–January 5, 2018), cycle number, and residuals (ETD) between observed and predicted times derived from the updated linear ephemeris (Equation 5).

HJD 2400000+	*HJD Error*	*Cycle No.*	*ETD[a]*	*Reference*
52742.6100	—[c]	–14270	–0.02885	Greaves and Wils 2003
55164.7680	—[c]	–7847	–0.00574	Diethelm 2011
55564.8728[b]	0.0002	–6786	–0.00761	Diethelm 2011
55989.6866	0.0005	–5659.5	–0.00074	Diethelm 2012
56726.3599	0.0005	–3706	0.00114	Hübscher and Lehmann 2015
58110.8940	0.0002	–34.5	0.00023	This study
58115.7964	0.0002	–21.5	0.00030	This study
58115.9840	0.0003	–21	–0.00069	This study
58116.9276	0.0002	–18.5	0.00017	This study
58117.8696	0.0001	–16	–0.00056	This study
58118.8126	0.0001	–13.5	–0.00030	This study
58123.9043	0.0001	0	0.00047	This study

a. ETD = Eclipse Time Difference between observed time of minimum and those calculated using the updated ephemeris (Equation 5).
b. Outlier value shown as an asterisk in Figure 3 not included in period analyses.
c. Not reported.

Table 4. Estimation of effective temperature (T_{eff1}) of V647 Vir based upon dereddened (B–V) data from five surveys and the present study.

	USNO-B1.0	*USNO-A2.0*	*2MASS*	*SDSS-DR8*	*UCAC4*	*Present Study*
$(B–V)_0$[a]	0.500	0.704	0.682	0.814	0.703	0.679
T_{eff1}[b] (K)	6278	5590	5653	5283	5594	5663
Spectral Class[b]	F6V-F7V	G5V-G6V	G5V-G6V	G9V-K0V	G5V-G6V	G4V-G5V

a. Intrinsic $(B–V)_0$ determined using reddening value E(B–V) = 0.023 ± 0.001.
b. T_{eff1} interpolated and spectral class range estimated from Pecaut and Mamajek (2013). Median value, $(B–V)_0$ = 0.693 ± 0.012, corresponds to a G5V-G6V primary star (T_{eff1} = 5620 ± 102 K).

reference epoch (Kreiner 2004) defined by the following linear ephemeris (Equation 3):

$$\text{Min I (HJD)} = 2455164.7622 + 0.3771061\ \text{E}. \quad (3)$$

Plotting (Figure 3) the difference between the observed eclipse times and those predicted by the linear ephemeris against epoch (cycle number) uncovered what appears to be a quadratic relationship (Equation 4) where:

$$\text{ETD} = -4.8328 \cdot 10^{-5} - 1.0266 \cdot 10^{-6}\,\text{E} - 2.1387 \cdot 10^{-10}\,\text{E}^2. \quad (4)$$

In this case the ETD residuals vs. epoch can be best described by an expression with a negative quadratic coefficient ($-2.1387 \cdot 10^{-10}$) suggesting that the orbital period has been slowly decreasing over time at the rate of 0.0358 (13) $s \cdot y^{-1}$.

An updated linear ephemeris (Equation 5) based on near term ETD values (2012–2018) was calculated as follows:

$$\text{Min I (HJD)} = 2458123.9038\ (3) + 0.3771034\ (1)\ \text{E}. \quad (5)$$

These data are shown as a horizontal line within the inset for Figure 3. Nevertheless, since the orbital period appears to be decreasing linearly with time, ephemerides for V948 Mon will need to be updated on a regular basis.

3.2. Effective temperature estimation

Throughout this paper the primary star is defined as the hotter and more massive member of each binary system. No classification spectra are published for either W UMa-type variable so that the effective temperature (T_{eff1}) of each primary star has been estimated using color index (B–V) data acquired at DBO and others determined from astrometric (USNO-A2.0, USNO-B1.0, and UCAC4) and photometric (2MASS, SDSS-DR8, and APASS) surveys. Interstellar extinction (A_V) was calculated (E (B–V) × 3.1) using the reddening value (E (B–V)) estimated from Galactic dust map models reported by Schlafly and Finkbeiner (2011).

Intrinsic color ($(B–V)_0$) for V647 Vir that was calculated from measurements made at DBO and those acquired from five other sources are listed in Table 4. The median value (0.693 ± 0.012) which was adopted for Roche modeling indicates a primary star with an effective temperature (5620 ± 102 K) that probably ranges in spectral class between G5V and G6V. This result is nearly identical to the Gaia DR2 release of stellar parameters (Andrae *et al.* 2018) in which the T_{eff} for V647 Vir is reported to be 5620^{+36}_{-240} K.

Table 5. Estimation of effective temperature (Teff1) of V948 Mon based upon dereddened (B-V) data from six surveys and the present study.

	USNO-B1.0	*USNO-A2.0*	*2MASS*	*SDSS-DR8*	*UCAC4*	*APASS*	*Present Study*
$(B–V)_0$ [a]	0.931	0.646	0.447	0.845	0.445	0.445	0.428
T_{eff1} [b] (K)	4962	5779	6477	5179	6483	6483	6560
Spectral Class[b]	K2V-K3V	G1V-G2V	F5V-F6V	K0V-K1V	F5V-F6V	F5V-F6V	F5V-F6V

a. Intrinsic $(B–V)_0$ determined using reddening value E(B–V) = 0.028 ± 0.001.

b. T_{eff1} interpolated and spectral class range estimated from Pecaut and Mamajek (2013). Median value, $(B–V)_0$ = 0.447 ± 0.019, corresponds to an F3V-F7V primary star (T_{eff1} = 6480 ± 274 K).

Similarly, dereddened color indices ($(B–V)_0$) for V948 Mon from different sources are listed in Table 5. The median value (0.447±0.019) adopted for Roche modeling corresponds to a primary star with an effective temperature (6480±270 K) that likely ranges in spectral class between F3V and F7V. The median result is somewhat higher than the value reported in the Gaia DR2 release of stellar parameters (Andrae *et al.* 2018) but well within the documented confidence intervals ($T_{eff} = 6337^{+418}_{-168}$ K).

3.3. Roche modeling approach

Roche modeling of LC data from V647 Vir and V948 Mon was primarily accomplished using the programs PHOEBE 0.31a (Prša and Zwitter 2005) and WDWINT56A (Nelson 2009). Both feature an easy-to-use GUI interface to the Wilson-Devinney WD 2003 code (Wilson and Devinney 1971; Wilson 1979, 1990). WDWINT56A makes use of Kurucz's atmosphere models (Kurucz 2002) which are integrated over BVR_cI_c optical passbands. In both cases, the selected model was Mode 3 for an overcontact binary. Other modes (detached and semi-detached) were explored but never approached the goodness of fit achieved with Mode 3. Since the internal energy transfer to the surface of both variable systems is driven by convective (<7500 K) rather than radiative processes, the value for bolometric albedo ($A_{1,2}$=0.5) was assigned according to Ruciński (1969) while the gravity darkening coefficient ($g_{1,2}$=0.32) was adopted from Lucy (1967). Logarithmic limb darkening coefficients (x_1, x_2, y_1, y_2) were interpolated (Van Hamme 1993) following each change in the effective temperature (T_{eff2}) of the secondary star during model fit optimization using differential corrections (DC). All but the temperature of the more massive star (T_{eff1}), $A_{1,2}$, and $g_{1,2}$ were allowed to vary during DC iterations. In general, the best fits for T_{eff2}, i, q, and Roche potentials ($\Omega_1 = \Omega_2$) were collectively refined (method of multiple subsets) by DC using the multicolor LC data. LCs from V647 Vir (Figures 4 and 5) and V948 Mon (Figure 6) do not exhibit significant asymmetry during quadrature (Max. I ≅ Max. II) which is often attributed to the so-called O'Connell effect (O'Connell 1951). No spots were introduced during Roche modeling of V948 Mon, however, a cool spot was necessary to achieve the best fit of LC data for V647 Vir during Min II (Figure 5). Third light contribution (l_3) during DC optimization did not lead to any value significantly different from zero with either binary system. Since both systems clearly undergo a total eclipse during Min II, Roche model convergence to a unique value for q should be self-evident. To make this point and also to demonstrate that both systems are most likely A-type overcontact variables, a grid search was

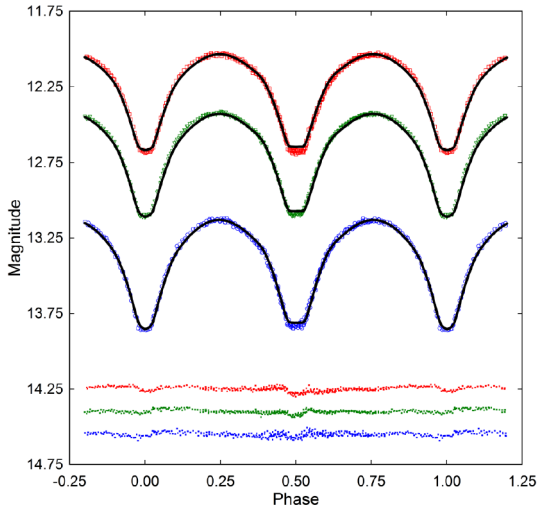

Figure 4. Folded CCD light curves for V647 Vir produced from photometric data obtained between January 25, 2018 and March 19, 2018. The top (I_c), middle (V), and bottom curve (B) shown above were reduced to APASS-based catalog magnitudes using MPO CANOPUS (Minor Planet Observer 2010). In this case, the Roche model assumed an A-type overcontact binary with no spots; residuals from the model fits are offset at the bottom of the plot to keep the values on scale.

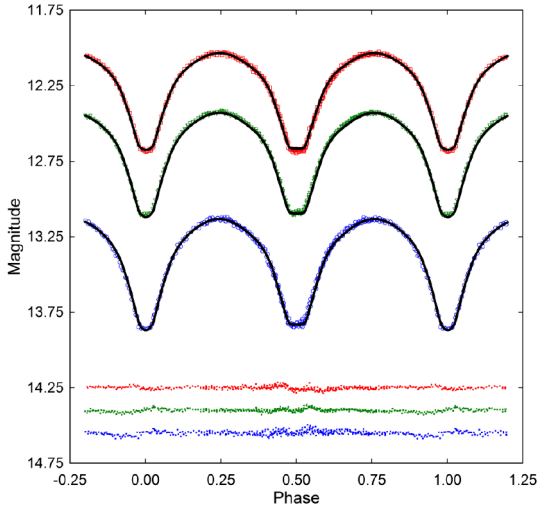

Figure 5. Folded CCD light curves for V647 Vir produced from photometric data obtained between January 25, 2018 and March 19, 2018. The top (I_c), middle (V), and bottom curve (B) shown above were reduced to APASS-based catalog magnitudes using MPO CANOPUS (Minor Planet Observer 2010). In this case, the Roche model assumed an A-type overcontact binary with a cool spot on the primary star; residuals from the model fits are offset at the bottom of the plot to keep the values on scale.

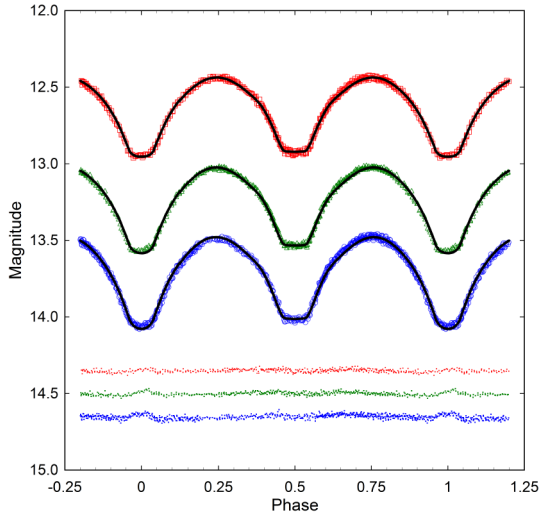

Figure 6. Folded CCD light curves for V948 Mon produced from photometric data obtained between December 23, 2017 and January 5, 2018. The top (I_c), middle (V), and bottom curve (B) shown above were reduced to APASS-based catalog magnitudes using MPO CANOPUS (Minor Planet Observer 2010). In this case, the Roche model assumed an A-type overcontact binary with no spots; residuals from the model fits are offset at the bottom of the plot to keep the values on scale.

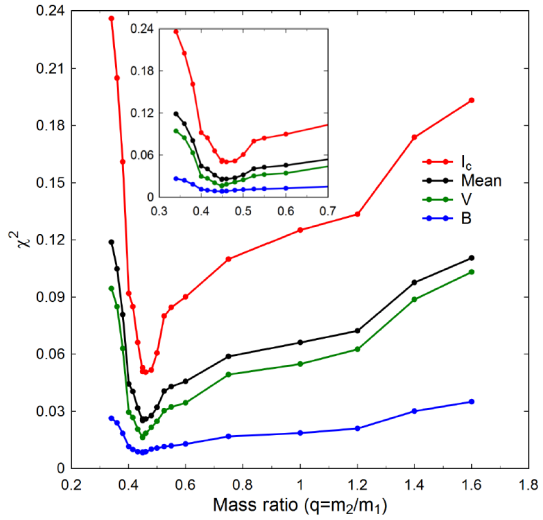

Figure 7. V647 Vir Roche model fit error minimization (χ^2) from PHOEBE 0.31a (Prša and Zwitter 2005) using the "q-search" approach. The figure inset zooms in where the best fit for q (~0.45) is observed.

performed on V647 Vir (Figure 7) and V948 Mon (Figure 8) by fixing the mass ratio at various intervals and finding a best fit for (T_{eff2}, i, and $\Omega_1 = \Omega_2$) using DC. These results are described in more detail within the subsections for each variable that follow.

3.4. Roche modeling results

Without radial velocity (RV) data, it is not possible to unambiguously determine the mass ratio or total mass. The total eclipse observed in the LCs from both systems greatly improves the chances of finding a unique mass ratio value for each star. Still, there is some risk at attempting to establish a mass ratio (q_{ptm}) with photometric data alone (Terrell and Wilson 2005). Standard errors reported in Tables 6–8 are computed from the DC covariance matrix and only reflect the model fit to the

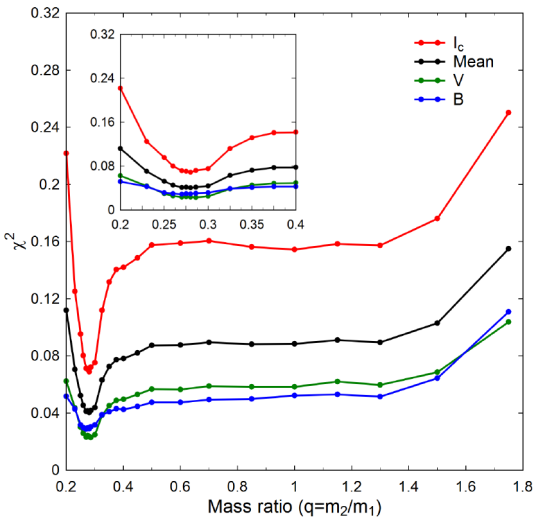

Figure 8. V948 Mon Roche model fit error minimization (χ^2) from PHOEBE 0.31a (Prša and Zwitter 2005) using the "q-search" approach. The figure inset zooms in where the best fit for q (~0.28) is observed.

observations which assume exact values for any fixed parameter. These intra-study errors may appear unrealistically small considering the estimated uncertainties associated with the mean adopted T_{eff1} values (Tables 6–8) along with basic assumptions about $A_{1,2}$, $g_{1,2}$, and the influence of spots added to the Roche model. Alternative approaches to locate the best Roche model fit in a multi-parameter space which have gained popularity include simplex optimization and heuristic scanning (also known as Monte Carlo simulation). Nonetheless, as discussed in more detail by Wilson and Van Hamme (2016), there is nothing inherently wrong with using DC for parameter estimation and determination of standard errors. Furthermore, Abubekerov *et al.* (2008, 2009) argue that for significantly nonlinear multi-parameter relationships the standard errors produced from DC or Monte-Carlo simulations are nearly equivalent. One normally fixes the value for T_{eff1} during modeling with the WD code despite acknowledging measurement uncertainty which can easily approach ±400 K. To address this concern, the effect that adjusting T_{eff1} would have on modeling estimates for q, i, $\Omega_{1,2}$, T_{eff2} along with the putative cool spot on V647 Vir was explored (Tables 6–8). In order to maximize the possibility of observing an effect, the worst case estimates for V647 Vir (5620±240 K) and V948 Mon (6480±418 K) obtained from Gaia DR2 were used for this analysis. Interestingly, with the obvious exception of T_{eff2}, varying T_{eff1} did not appreciably affect the model estimates (R.S.D. < 2%) for i, q, or $\Omega_{1,2}$ (Tables 6–8). Said another way, assuming that the true T_{eff1} for V647 Vir falls within 5620±240 K and that for V948 Mon within 6480±418 K, the model fits for both systems were relatively insensitive to the T_{eff1}. These findings are consistent with similar results reported for AR CrB (Alton and Nelson 2018), a W-type overcontact binary in which T_{eff1} was tested over an even wider (±3σ) range.

The fill-out parameter (f) which corresponds to the outer surface shared by each star was calculated according to Equation 6 (Kallrath and Malone 1999; Bradstreet 2005) where:

$$f = (\Omega_{inner} - \Omega_{1,2}) / (\Omega_{inner} - \Omega_{outer}). \quad (6)$$

Table 6. V647 Vir lightcurve parameters evaluated by Roche modeling and the geometric elements derived for V647 Vir assuming it is an A-type W UMa variable with no spots. Modeling estimates also include those determined at the uncertainty boundaries (T_{eff1} = 5620 ± 240 K) for the primary star.

Parameter	*No spot*	*No spot*	*No spot*	*Mean*
T_{eff1} (K)[b]	5380	5620	5860	5620
T_{eff2} (K)	5499 (1)	5743 (2)	5974 (1)	5739 (238)
q (m_2 / m_1)	0.449 (1)	0.449 (1)	0.458 (1)	0.452 (5)
A[b]	0.5	0.5	0.5	0.5
g[b]	0.32	0.32	0.32	0.32
$\Omega_1 = \Omega_2$	2.742 (1)	2.738 (2)	2.754 (1)	2.745 (8)
i°	86.3 (2)	87.47 (8)	89.3 (8)	87.7 (1.5)
$L_1 / (L_1 + L_2)_B$[c]	0.6420 (2)	0.6435 (2)	0.6435 (2)	0.6430 (9)
$L_1 / (L_1 + L_2)_V$	0.6501 (1)	0.6515 (1)	0.6504 (1)	0.6507 (7)
$L_1 / (L_1 + L_2)_{Ic}$	0.6568 (2)	0.6576 (2)	0.6559 (2)	0.6568 (9)
r_1 (pole)	0.4292 (2)	0.4300 (3)	0.4286 (2)	0.4293 (7)
r_1 (side)	0.4582 (3)	0.4592 (4)	0.4577 (3)	0.4584 (8)
r_1 (back)	0.4880 (4)	0.4893 (5)	0.4880 (4)	0.4884 (8)
r_2 (pole)	0.2975 (3)	0.2983 (3)	0.3003 (3)	0.2987 (14)
r_2 (side)	0.3113 (3)	0.3122 (4)	0.3143 (3)	0.3126 (15)
r_2 (back)	0.3481 (5)	0.3497 (6)	0.3520 (5)	0.3499 (20)
Fill-out factor (%)	12.4	14.0	14.5	13.6 (1.1)
SSR (B)[d]	0.0280	0.0296	0.0272	0.0283 (12)
SSR (V)[d]	0.0146	0.0198	0.0156	0.0167 (28)
SSR (Ic)[d]	0.0342	0.0342	0.0321	0.0328 (12)

a. All error estimates for T_{eff2}, q, $\Omega_{1,2}$, i, $r_{1,2}$, and L_1 from WDWINT56A *(Nelson 2009).*
b. Fixed during DC.
c. L_1 and L_2 refer to scaled luminosities of the primary and secondary stars, respectively.
d. Monochromatic sum of squares residual fit from observed values.

Table 7. V647 Vir lightcurve parameters evaluated by Roche modeling and the geometric elements derived for V647 Vir assuming it is an A-type W UMa variable with a cool spot on the primary star. Modeling estimates also include those determined at the uncertainty boundaries (T_{eff1} = 5620 ± 240 K) for the primary star.

Parameter	*Spotted*	*Spotted*	*Spotted*	*Mean*
T_{eff1} (K)[b]	5380	5620	5860	5620
T_{eff2} (K)	5419 (1)	5607 (1)	5843 (2)	5623 (212)
q (m_2 / m_1)	0.460 (1)	0.466 (1)	0.468 (1)	0.465 (2)
A[b]	0.5	0.5	0.5	0.5
g[b]	0.32	0.32	0.32	0.32
$\Omega_1 = \Omega_2$	2.776 (3)	2.796 (1)	2.793 (1)	2.788 (11)
i°	86.8 (2)	86.2 (2)	88.24 (77)	87.1 (1.1)
$A_S = T_S / T_\star$[c]	0.80 (1)	0.78 (1)	0.77 (1)	0.78 (2)
Θ_S(spot co-latitude)[c]	90 (6)	90 (6)	90 (4)	90 (3)
φ_S (spot longitude)[c]	180 (1)	180 (1)	180 (1)	180 (1)
r_S (angular radius)[c]	10.0 (1)	12.0 (1)	12.0 (1)	11.3 (1.2)
$L_1 / (L_1 + L_2)_B$[d]	0.6590 (2)	0.6705 (2)	0.6702 (2)	0.6666 (65)
$L_1 / (L_1 + L_2)_V$	0.6620 (1)	0.6699 (1)	0.6693 (1)	0.6671 (44)
$L_1 / (L_1 + L_2)_{Ic}$	0.6643 (2)	0.6693 (2)	0.6686 (2)	0.6674 (27)
r_1 (pole)	0.4251 (2)	0.4226 (3)	0.4233 (2)	0.4237 (13)
r_1 (side)	0.4531 (4)	0.4500 (4)	0.4510 (3)	0.4514 (16)
r_1 (back)	0.4822 (5)	0.4786 (4)	0.4800 (4)	0.4803 (18)
r_2 (pole)	0.2973 (10)	0.2970 (9)	0.2983 (2)	0.2975 (7)
r_2 (side)	0.3108 (12)	0.3102 (12)	0.3118 (3)	0.3109 (8)
r_2 (back)	0.3460 (20)	0.3445 (19)	0.3468 (4)	0.3458 (12)
Fill-out factor (%)	8.1	5.2	7.3	6.9 (1.5)
SSR (B)[e]	0.0259	0.0265	0.0253	0.0259 (6)
SSR (V)[e]	0.0128	0.0131	0.0121	0.0127 (5)
SSR (I_c)[e]	0.0236	0.0222	0.0214	0.0224 (11)

a. All error estimates for T_{eff2}, q, i, $\Omega_{1,2}$, A_S, Θ_S, φ_S, r_S, $r_{1,2}$, and L_1 from WDWINT56A *(Nelson 2009).*
b. Fixed during DC.
c. Temperature factor (A_S); location (Θ_S, φ_S) and size (r_S) parameters in degrees.
d. L_1 and L_2 refer to scaled luminosities of the primary and secondary stars, respectively.
e. Monochromatic sum of squares residual fit from observed values.

Ω_{outer} is the outer critical Roche equipotential, Ω_{inner} is the value for the inner critical Roche equipotential, and $\Omega = \Omega_{1,2}$ denotes the common envelope surface potential for the binary system. In both cases the systems are considered overcontact since $0 < f < 1$.

3.4.1. V647 Vir

LC parameters and geometric elements derived from the WD code are summarized in Table 6 (no spot) and Table 7 (cool spot). According to Binnendijk (1970) the deepest minimum (Min I) of an A-type overcontact system occurs when the hotter and larger star is occulted by the cooler less massive member of the binary system. With V647 Vir, the flat-bottomed dip in brightness indicative of a total eclipse of the secondary occurs at Min II while the round-bottomed deeper minimum (Min I) results from a transit across the primary face. As expected, the "q-search" results (Figure 7) clearly illustrate that model error quickly reaches a minimum as the mass ratio approaches ~0.45. It is also evident that V647 Vir is most likely an A-type overcontact binary; consequently, WD modeling proceeded under this assumption. Min II from the I_c-band LC includes two data points that are slightly deeper (<0.012 mag) than Min I, which could indicate that V647 Vir is a W-type system. Attempts to simultaneously model all LC data under this assumption (q≃2.22 and fixed values for T_{eff2}) produced grossly misshaped fits and were thereafter abandoned. Instead, adding a cool spot to the WD model improved the light curve fits during Min II (Figure 5), which resulted in lower sum of squared residuals (SSR) compared to the unspotted fit (Tables 6 and 7). A three-dimensional image rendered (Figure 9) using BINARYMAKER3 (BM3; Bradstreet and Steelman 2004) illustrates the transit during Min I (φ=0) and the cool spot location on the primary star (φ=0.60).

It could be argued in some cases that an A-type system is a cool or hot spot away from being classified as a W-type overcontact binary (and vice-versa). Inspection of the sparsely sampled ASAS and NSVS survey data folded with high cadence V-mag data from DBO (Figure 1) suggests that there is significant variability in the depth of Min II. Also, it should be noted that contrary to expectations for an A-type system, the best fit of the unspotted LC data occurred when the effective temperature of the secondary star (T_{eff2}) was higher (114–119 K) than the primary (T_{eff1}) component (Table 6). Not without precedence, this phenomenon has also been observed for EK Com (Deb *et al.* 2010), HV Aqr (Gazeas *et al.* 2007), BO CVn (Zola *et al.* 2012), and TYC 1664-0110-1 (Alton and Stępień 2016). It is therefore not unreasonable to propose that V647 Vir has in the past or will at some future date give the appearance of a W-type overcontact system.

3.4.2. V948 Mon

The broad flattened bottom (Figure 6) observed during Min II is a diagnostic indicator for a total eclipse of the secondary star. It follows that minimum light (Min I) occurs when the smaller secondary transits the primary star. As shown

Table 8. V984 Mon lightcurve parameters evaluated by Roche modeling and the geometric elements derived for V948 Mon assuming it is an A-type W UMa variable. Modeling estimates also include those determined at the uncertainty boundaries (T_{eff1} = 6480 ± 418 K) for the primary star.

Parameter	*No spot*	*No spot*	*No spot*	*Mean*
T_{eff1} (K)[b]	6062	6480	6898	6480
T_{eff2} (K)	6100 (2)	6505 (4)	6926 (2)	6510 (413)
q (m_2 / m_1)	0.283 (1)	0.286 (1)	0.287 (1)	0.285 (2)
A[b]	0.5	0.5	0.5	0.5
g[b]	0.32	0.32	0.32	0.32
$\Omega_1 = \Omega_2$	2.342 (2)	2.347 (3)	2.342 (1)	2.344 (3)
i°	86.5 (4)	88.2 (8)	87.3 (3)	87.3 (9)
$L_1 / (L_1 + L_2)_B$[c]	0.7410 (2)	0.7414 (2)	0.7389 (2))	0.7404 (13)
$L_1 / (L_1 + L_2)_V$	0.7431 (1)	0.7427 (1)	0.7403(1)	0.7420 (15)
$L_1 / (L_1 + L_2)_{Ic}$	0.7448 (1)	0.7440 (2)	0.7420 (1)	0.7436 (14)
r_1 (pole)	0.4792 (3)	0.4787 (5)	0.4799 (2)	0.4793 (6)
r_1 (side)	0.5218 (4)	0.5212 (6)	0.5229 (3)	0.5220 (9)
r_1 (back)	0.5535 (6)	0.5531 (7)	0.5555 (4)	0.5540 (13)
r_2 (pole)	0.2773 (3)	0.2786 (15)	0.2803 (3)	0.2787 (15)
r_2 (side)	0.2919 (4)	0.2933 (18)	0.2954 (3)	0.2935 (18)
r_2 (back)	0.3458 (9)	0.3477 (43)	0.3521 (7)	0.3485 (32)
Fill-out factor (%)	52.2	49.2	51.0	51.1 (1.6)
SSR (B)[d]	0.0631	0.0625	0.0611	0.0623 (11)
SSR (V)[d]	0.0210	0.0208	0.0203	0.0207 (4)
SSR (I_c)[d]	0.0224	0.0227	0.0220	0.0224 (3)

a. All error estimates for T_{eff2}, q, i, $\Omega_{1,2}$, $r_{1,2}$, and L_1 from WDWINT56A (Nelson 2009).
b. Fixed during DC.
c. L_1 and L_2 refer to scaled luminosities of the primary and secondary stars, respectively.
d. Monochromatic sum of squares residual fit from observed values.

Table 9. Fundamental stellar parameters for V647 Vir using the mean photometric mass ratio ($q_{ptm} = m_2 / m_1$) from the spotted Roche model fits of LC data (2018) and the estimated mass for a putative G5V-G6V primary star in a W UMa variable.

Parameter	*Primary*	*Secondary*
Mass ($M_\odot$)	1.13 ± 0.05	0.53 ± 0.02
Radius ($R_\odot$)	1.10 ± 0.01	0.78 ± 0.01
a ($R_\odot$)	2.46 ± 0.03	2.46 ± 0.03
Luminosity ($L_\odot$)	1.09 ± 0.03	0.54 ± 0.01
M_{bol}	4.66 ± 0.03	5.43 ± 0.03
Log (g)	4.41 ± 0.02	4.38 ± 0.02

Table 10. Fundamental stellar parameters for V948 Mon using the mean photometric mass ratio ($q_{ptm} = m_2 / m_1$) from the spotted Roche model fits of LC data (2017–2018) and the estimated mass for a putative F3V-F7V primary star in a W UMa variable.

Parameter	*Primary*	*Secondary*
Mass ($M_\odot$)	1.32 ± 0.07	0.38 ± 0.02
Radius ($R_\odot$)	1.28 ± 0.02	0.73 ± 0.01
a ($R_\odot$)	2.62 ± 0.04	2.62 ± 0.04
Luminosity ($L_\odot$)	2.61 ± 0.07	0.85 ± 0.02
M_{bol}	3.71 ± 0.03	4.93 ± 0.03
Log (g)	4.34 ± 0.03	4.29 ± 0.03

in Figure 8, model error quickly reaches a minimum as the mass ratio approaches ~0.28. In this regard V948 Vir behaves like an A-type overcontact binary and was therefore modeled according to this assumption. The Roche model for V948 Mon did not require the addition of a spot to improve the LC fits. LC parameters and geometric elements derived from the WD code are summarized in Table 8. Similar to V647 Vir, the best fit of V948 Mon LC data occurred when the effective temperature of the secondary star (T_{eff2}) was slightly higher (25–38 K) than the primary (T_{eff1}) component. In this regard, attempts to model V948 Mon as a W-type overcontact system also proved unsuccessful. A three-dimensional rendering produced using BM3 (Figure 10) shows the transit during Min I (φ = 0) and the Roche lobe surface outline (φ = 0.75).

3.5. Absolute parameters

Fundamental stellar parameters were estimated for both binary stars using results from the best fit simulations of the 2018 LCs. However, without the benefit of RV data and classification spectra, these results should be more accurately described as "relative" rather than "absolute" parameters and considered preliminary in that regard.

3.5.1. V647 Vir

Gazeas and Stępień (2008) noted that primary (defined as more the massive component) stars in cool contact binaries obey the mass-radius relation associated with main-sequence (MS) stars. Power-law fits for the primary radii correspond very closely to those determined from single MS stars with masses lower than 1.8 $M_\odot$ (Giménez and Zamorano 1985). Therefore, reasonable estimates for the mass and radius of a primary star (most often populated by a MS star) in a W UMa-type binary system can be derived using data published for MS stars. These tabulations cover a wide range of spectral types typically attributed to primary stars in an overcontact binary system. For a putative G5V-G6V system (T_{eff1} ~ 5620 K) like V647 Vir, this includes a value ($M_1 = 1.07 \pm 0.05\ M_\odot$) interpolated from Harmanec (1988) and another ($M_1 = 0.98 \pm 0.02\ M_\odot$) from Pecaut and Mamajek (2013). A final relationship reported by Torres *et al.* (2010) for main sequence stars above 0.6 $M_\odot$ predicts a mass of 1.03 $M_\odot$ for the primary component. Importantly, three different empirically derived mass-period relationships for W UMa binaries have been published by Qian (2003) then later by Gazeas and Stępień (2008) and Gazeas (2009). According to Qian (2003) when the primary star is less than 1.35 $M_\odot$ its mass can be determined from Equation 7:

$$\log M_1 = 0.391\ (59) \log P + 1.96\ (17), \quad (7)$$

or alternatively when $M_1 > 1.35\ M_\odot$ then Equation 8:

$$\log M_1 = 0.761\ (150) \log P + 1.82\ (28), \quad (8)$$

where P is the orbital period in days. Using Equation 7 leads to M_1 = 1.07 ± 0.08 $M_\odot$ for the primary. The mass-period relationship (Equation 9) derived by Gazeas and Stępień (2008):

$$\log M_1 = 0.755\ (59) \log P + 0.416\ (24), \quad (9)$$

corresponds to a W UMa system where $M_1 = 1.17 \pm 0.10\ M_\odot$. Gazeas (2009) reported another empirical relationship (Equation 10) for the more massive (M_1) star of a contact binary such that:

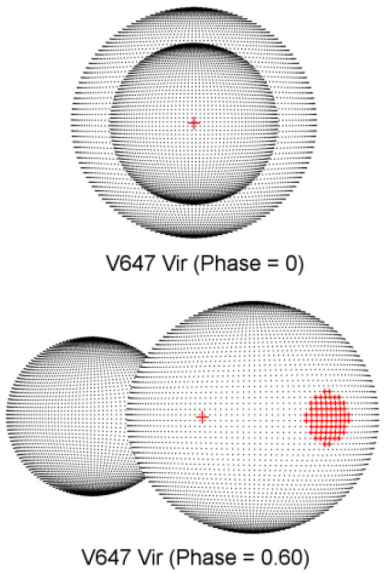

Figure 9. Three-dimensional spatial model of V647 Vir illustrating the transit of the secondary star across the primary star face at Min I (φ = 0) and cool spot location (φ = 0.60) on the primary star.

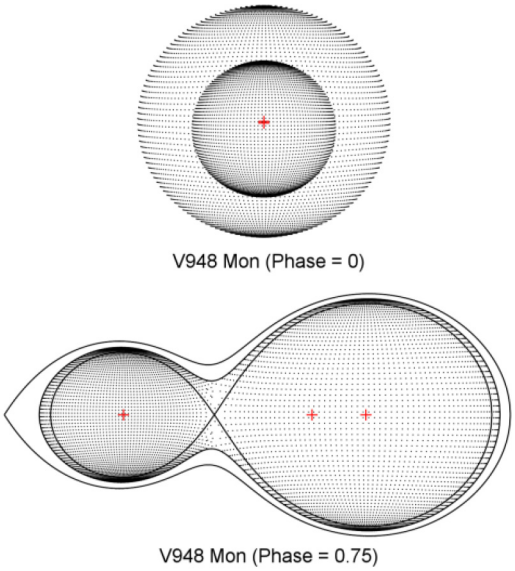

Figure 10. Three-dimensional spatial model of V948 Mon showing the transit at Min I (φ = 0) and the Roche lobe surface outline (φ = 0.75).

$$\log M_1 = 0.725\ (59) \log P - 0.076\ (32) \log q + 0.365\ (32), \quad (10)$$

in which $M_1 = 1.14 \pm 0.08\ M_\odot$. The mean of three values (M_1 = 1.13 ± 0.05 $M_\odot$) estimated from empirical models (Equations 7, 9, and 10) for W UMa binaries was used for subsequent determinations of M_2, semi-major axis a, volume-radii r_L, and bolometric magnitudes (M_{bol}) for V647 Vir. The mass estimates from Harmanec (1988), Pecaut and Mamajek (2013), and Torres (2010) are interesting in that they reflect values expected from single stars. In this case a single G5V-G6V star was estimated to be less massive (1.02 ± 0.05 $M_\odot$) than the primary star in V647 Vir. The secondary mass (0.53 ± 0.02 $M_\odot$) and total mass (1.66 ± 0.06 $M_\odot$) of the system were subsequently determined using the mean photometric mass ratio (0.465 ± 0.002) from the spotted Roche model. By comparison, a single main sequence star with a mass similar to the secondary (late K-type) would likely be much smaller ($R_\odot \sim 0.55$), cooler ($T_{eff} \sim 4000$), and far less luminous ($L_\odot \sim 0.07$). The semi-major axis, $a(R_\odot) = 2.46 \pm 0.03$, was calculated from Newton's version (Equation 11) of Kepler's third law where:

$$a^3 = (G \times P^2\ (M_1 + M_2)) / (4\pi^2). \quad (11)$$

The effective radius of each Roche lobe (r_L) can be calculated over the entire range of mass ratios ($0 < q < \infty$) according to an expression (Equation 12) derived by Eggleton (1983):

$$r_L = (0.49q^{2/3}) / (0.6q^{2/3} + ln(1 + q^{1/3})), \quad (12)$$

from which values for r_1 (0.4462±0.0002) and r_2 (0.3152±0.0002) were determined for the primary and secondary stars, respectively. Since the semi-major axis and the volume radii are known, the radii in solar units for both binary components can be calculated where $R_1 = a \cdot r_1 = 1.10 \pm 0.01\ R_\odot$ and $R_2 = a \cdot r_2 = 0.78 \pm 0.01\ R_\odot$.

Luminosity in solar units ($L_\odot$) for the primary (L_1) and secondary stars (L_2) was calculated from the well-known relationship (Equation 13) where:

$$L_{1,2} = (R_{1,2} / R_\odot)2\ (T_{1,2} / T_\odot)^4. \quad (13)$$

Assuming that $T_{eff1} = 5620$ K, $T_{eff2} = 5607$ K, and $T_\odot = 5772$ K, then the solar luminosities ($L_\odot$) for the primary and secondary are L_1 = 1.09 ± 0.02 and L_2 = 0.54 ± 0.01, respectively. According to the Gaia DR2 release of stellar parameters (Andrae *et al.* 2018), the reported T_{eff} (5620^{+36}_{-240} K) is nearly identical to the adopted T_{eff1} (5620 K) value while the size ($R_\odot$ = 1.21) and luminosity ($L_\odot$ = 1.32) of the primary star in V647 Vir are greater than the corresponding values generated by the study herein. Based on the Bailer-Jones (2015) correction for parallax data in Gaia DR2 (Gaia *et al.* 2016, 2018) this system can be found at a distance of $444.5^{+8.2}_{-7.9}$ pc. By comparison, a value derived using the distance modulus equation corrected for interstellar extinction (A_V = 0.070 ± 0.003) places V647 Vir slightly farther (471 ± 7 pc) away. Other values derived herein and necessary to perform this calculation include V_{avg} = 12.77 ± 0.01, bolometric correction (BC = –0.14), $A_V = 0.070 \pm 0.002$, and the absolute V-magnitude ($M_V = 4.33 \pm 0.03$) from the combined luminosity (4.19 ± 0.03).

3.5.2. V948 Mon

The same approach described above for V647 Vir was used to estimate the primary star mass for V948 Mon (Table 8) but this time for a putative F3V-F7V system ($T_{eff1} \sim 6480$ K). The mass-period empirical relationships (Equations 8–10) lead to a mean value of $M_1 = 1.32 \pm 0.07\ M_\odot$ for the primary star. Interestingly, this was nearly identical ($M_1 = 1.31 \pm 0.04\ M_\odot$) to that obtained from single star estimates for an F3V-F7V system. The secondary mass = 0.38 ± 0.02 $M_\odot$ and total mass (1.69 ± 0.07 $M_\odot$) of the system were derived from the mean photometric mass ratio (0.285 ± 0.002). If the secondary was a single main sequence star with a similar mass (early M-type) it would probably be much smaller ($R_\odot \sim 0.42$), cooler ($T_{eff} \sim 3600$), and

far less luminous ($L_\odot \sim 0.03$). The semi-major axis, $a(R_\odot) = 2.62 \pm 0.04$, was calculated from Equation 11 while the effective radius of each Roche lobe (r_L) was calculated according to Equation 12 from which values for r_1 (0.4898 ± 0.0006) and r_2 (0.2773 ± 0.0005) were determined for the primary and secondary stars, respectively. The radii in solar units for both binary components were calculated such that $R_1 = 1.28 \pm 0.02$ $R_\odot$ and $R_2 = 0.73 \pm 0.01$ $R_\odot$. Luminosity in solar units ($L_\odot$) for the primary (L_1) and secondary stars (L_2) was calculated according to Equation 13. Assuming that $T_{eff1} = 6480$ K, $T_{eff2} = 6505$ K, and $T_\odot = 5772$ K, then the solar luminosities for the primary and secondary are $L_1 = 2.61 \pm 0.07$ and $L_2 = 0.85 \pm 0.02$, respectively. According to the Gaia DR2 release of stellar parameters (Andrae *et al.* 2018), the reported T_{eff} (6337^{+418}_{-168} K) is not meaningfully different from the adopted value ($T_{eff1} = 6480$ K) used herein which was based on intrinsic color. However, the size ($R_\odot$ =1.44) and luminosity ($L_\odot$ = 3.03) of the primary star in V948 Mon are greater than the values estimated by the study herein. This system is estimated to be $879.3^{+36.1}_{-33.4}$ pc away using the Bailer-Jones (2015) correction for parallax-derived distances reported in Gaia DR2 (Gaia *et al.* 2016, 2018). A value independently derived from the distance modulus equation using data generated herein ($V_{avg} = 13.30 \pm 0.01$, $A_V = 0.079 \pm 0.003$, BC = –0.042, and $M_V = 3.41 \pm 0.03$) places V948 Mon a similarly distant 901 ± 14 pc away.

4. Conclusions

Seven new times of minimum were observed for both V647 Vir and V948 Mon based on recent (2017–2018) CCD-derived LC data collected with B, V, and I_c filters. These along with other published values led to an updated linear ephemeris for each system. Potential changes in orbital period were assessed using differences between observed and predicted eclipse timings. A quadratic relationship was established with ETD values determined from V948 Mon, suggesting that the orbital period has been slowly decreasing at a rate of $0.0358 \text{ s} \cdot \text{y}^{-1}$. Both systems will require many more years of eclipse timing data to further substantiate any potential change(s) in orbital period. The adopted effective temperatures (T_{eff1}) for V647 Vir (5620 K) and V948 Mon (6480 K) based on intrinsic color indices ($(B–V)_0$) were well within the confidence intervals reported from the Gaia DR2 release of stellar characteristics (Andrae *et al.* 2018). Estimates for the primary star luminosity ($L_\odot$) and radii ($R_\odot$) in both systems were lower (10–20%) than those reported in Gaia DR2. It is not known at this time whether this finding is coincidental or the result of a systematic bias in either method of determination. Both A-type overcontact systems clearly exhibit a total eclipse which is most evident as a flattened bottom during Min II. Therefore the photometric mass ratios for V647 Mon (q = 0.465) and V948 Mon (q = 0.285) determined by Roche modeling should prove to be a reliable substitute for mass ratios derived from RV data. Nonetheless, spectroscopic studies (RV and classification spectra) will be required to unequivocally determine a mass ratio, total mass, and spectral class for both systems.

5. Acknowledgements

This research has made use of the SIMBAD database operated at Centre de Données astronomiques de Strasbourg, France. Time of minima data tabulated in the Variable Star Section of Czech Astronomical Society (B.R.N.O.) website proved invaluable to the assessment of potential period changes experienced by this variable star. In addition, the Northern Sky Variability Survey hosted by the Los Alamos National Laboratory, the International Variable Star Index maintained by the AAVSO, the Catalina Sky Survey Data Release 2 maintained at Caltech, and the ASAS Catalogue of Variable Stars were mined for photometric data. The diligence and dedication shown by all associated with these organizations is very much appreciated. This work also presents results from the European Space Agency (ESA) space mission Gaia. Gaia data are being processed by the Gaia Data Processing and Analysis Consortium (DPAC). Funding for the DPAC is provided by national institutions, in particular the institutions participating in the Gaia MultiLateral Agreement (MLA). The Gaia mission website is https://www.cosmos.esa.int/gaia. The Gaia archive website is https://archives.esac.esa.int/gaia. Last, but certainly not least, the selfless support of the editorial staff at *JAAVSO* and the anonymous referee who provided critical review of this paper is greatly appreciated.

References

Abubekerov, M. K., Gostev, N. Yu. and Cherepashchuk, A. M. 2008, *Astron. Rep.*, **52**, 99.

Abubekerov, M. K., Gostev, N. Yu. and Cherepashchuk, A. M. 2009, *Astron. Rep.*, **53**, 722.

Akerlof, C., *et al.* 2000, *Astron. J.*, **119**, 1901.

Alton, K. B., and Nelson, R. H. 2018, *Mon. Not. Roy. Astron. Soc.*, **479**, 3197.

Alton, K. B., and Stępień, K 2016, *Acta Astron.*, **66**, 357.

Andrae, R., *et al.* 2018, *Astron. Astrophys.*, **616A**, 8.

Applegate, J. H. 1992, *Astrophys. J.*, **385**, 621.

Bailer-Jones, C. A. L. 2015, *Publ. Astron. Soc. Pacific*, **127**, 994.

Binnendijk, L. 1970, *Vistas Astron.*, **12**, 217.

Berry, R., and Burnell, J. 2005, *The Handbook of Astronomical Image Processing*, 2nd ed., Willmann-Bell, Richmond, VA.

Bradstreet, D. H. 2005, in *The Society for Astronomical Sciences 24th Annual Symposium on Telescope Science*, The Society for Astronomical Sciences, Rancho Cucamonga, CA, 23.

Bradstreet, D. H., and Steelman, D. P. 2004, BINARY MAKER 3, Contact Software (http://www.binarymaker.com).

Deb, S., Singh, H. P., Seshadri, T. R., and Gupta, R. 2010, *New Astron.*, **15**, 662.

Diethelm, R. 2009, *Inf. Bull. Var. Stars*, No. 5894, 1.

Diethelm, R. 2011, *Inf. Bull. Var. Stars*, No. 5992, 1.

Diethelm, R. 2012, *Inf. Bull. Var. Stars*, No. 6029. 1.

Diffraction Limited. 2019, MAXIMDL v.6.13, image processing software (http://www.cyanogen.com).

Drake, A. J., *et al.* 2014, *Astrophys. J., Suppl. Ser.*, **213**, 9.

Eggleton, P. P. 1983, *Astrophys. J.*, **268**, 368.

Gaia Collaboration, *et al.* 2016, *Astron. Astrophys.*, **595A**, 1.

Gaia Collaboration, *et al.* 2018, *Astron. Astrophys.*, **616A**, 1.

Gazeas, K. D. 2009, *Commun. Asteroseismology*, **159**, 129.
Gazeas, K. D., Niarchos, P.G., and Zola, S. 2007, in *Solar and Stellar Physics Through Eclipses*, eds. O. Demircan, S. O. Selam, B. Albayrak, ASP Conf. Ser. 370, 279.
Gazeas, K., and Stępień, K. 2008, *Mon. Not. Roy. Astron. Soc.*, **390**, 1577.
Gettel, S. J., Geske, M. T., and McKay, T. A. 2006, *Astron. J.,* **131**, 621.
Giménez, A., and Zamorano, J. 1985, *Astrophys. Space Sci.*, **114**, 259.
Greaves, J., and Wils, P. 2003, *Inf. Bull. Var. Stars*, No. 5458, 1.
Harmanec, P. 1988, *Bull. Astron. Inst. Czechoslovakia*, **39**, 329.
Henden, A. A., Levine, S. E., Terrell, D., Smith, T. C., and Welch, D. L. 2011, *Bull. Amer. Astron. Soc.*, **43**, 2011.
Henden, A. A., and Stone, R. C. 1998, *Astron. J.*, **115**, 296.
Henden, A. A., Terrell, D., Welch, D., and Smith, T. C. 2010, *Bull. Amer. Astron. Soc.*, **42**, 515.
Henden, A. A., Welch, D. L., Terrell, D., and Levine, S. E. 2009, *Bull. Amer. Astron. Soc.*, **41**, 669.
Hoffman, D. I., Harrison, T. E., and McNamara, B. J. 2009, *Astron. J.*, **138**, 466.
Hübscher, J., and Lehmann, P. B. 2015, *Inf. Bull. Var. Stars*, No. 6149, 1.
Kallrath, J., and Milone, E. F. 1999, *Eclipsing Binary Stars: Modeling and Analysis*, Springer-New York.
Kreiner, J. M. 2004, *Acta Astron.*, **54**, 207.
Kurucz, R. L. 2002, *Baltic Astron.*, **11**, 101.
Kwee, K. K., and van Woerden, H. 1956, *Bull. Astron. Inst. Netherlands*, **12**, 327.
Lucy, L. B. 1967, *Z. Astrophys.*, **65**, 89.
Minor Planet Observer. 2010, MPO Software Suite (http://www.minorplanetobserver.com), BDW Publishing, Colorado Springs.
Nelson, R. H. 2009, WDWINT v.56a astronomy software (https://www.variablestarssouth.org/bob-nelson).
O'Connell, D. J. K. 1951, *Publ. Riverview Coll. Obs.*, **2**, 85.
Paunzen, E., and Vanmunster, T. 2016, *Astron. Nachr.*, **337**, 239.
Pecaut, M. J., and Mamajek, E. E. 2013, *Astrophys. J. Suppl. Ser.*, **208**, 9.
Pojmański, G., Pilecki, B., and Szczygiel, D. 2005, *Acta Astron.*, **55**, 275.
Prša, A., and Zwitter, T. 2005, *Astrophys. J.*, **628**, 426.
Qian, S.-B. 2003, *Mon. Not. Roy. Astron. Soc.*, **342**, 1260.
Ruciński, S. M. 1969, *Acta Astron.*, **19**, 245.
Schlafly, E. F., and Finkbeiner, D. P. 2011, *Astrophys. J.*, **737**, 103.
Schwarzenberg-Czerny, A. 1996, *Astrophys. J., Lett.*, **460**, L107.
Smith, T. C., Henden, A. A., and Starkey, D. R. 2011, in *The Society for Astronomical Sciences 30th Annual Symposium on Telescope Science*, The Society for Astronomical Sciences, Rancho Cucamonga, CA, 121.
Software Bisque. 2019, THESKYX PRO v.10.5.0 software (http://www.bisque.com).
Terrell, D., and Wilson, R. E. 2005, *Astrophys. Space Sci.*, **296**, 221.
Torres, G., Andersen, J., and Giménez, A. 2010, *Astron. Astrophys. Rev.*, **18**, 67.
Van Hamme, W. 1993, *Astron. J.*, **106**, 2096.
Vanmunster, T. 2018, PERANSO v.2.50, light curve and period analysis software, (http://www.cbabelgium.com/peranso).
Wilson, R. E. 1979, *Astrophys. J.*, **234**, 1054.
Wilson, R. E. 1990, *Astrophys. J.*, **356**, 613.
Wilson, R. E., and Devinney, E. J. 1971, *Astron. J.*, **143**, 1.
Wilson, R. E., and Van Hamme, W. 2016, "Computing Binary Star Observables" (ftp://ftp.astro.ufl.edu/pub/wilson/lcdc2015/ebdoc.6jun2016.pdf).
Wozniak, P. R., *et al.* 2004, *Astron. J.*, **127**, 2436.
Zola, S., Nelson, R. H., Senavci, H. V., Szymanski, T., Kuźmicz, A., Winiarski, M., and Jableka, D. 2012, *New Astron.*, **17**, 673.